Journal of Hazardous Materials 199–200 (2012) 410–417

Contents lists available at SciVerse ScienceDirect

Journal of Hazardous Materials

journal homepage: www.elsevier.com/locate/jhazmat

Ultrasound-assisted synthesis and visible-light-driven photocatalytic activity of Fe-incorporated TiO_2 nanotube array photocatalysts

Qi Wu [a], Junjie Ouyang [a], Kunpeng Xie [a], Lan Sun [a,*], Mengye Wang [a], Changjian Lin [a,b]

[a] Department of Chemistry, College of Chemistry and Chemical Engineering, Xiamen University, Xiamen 361005, PR China
[b] State Key Laboratory of Physical Chemistry of Solid Surfaces, Xiamen University, Xiamen 361005, PR China

ARTICLE INFO

Article history:
Received 14 August 2011
Received in revised form 16 October 2011
Accepted 8 November 2011
Available online 15 November 2011

Keywords:
TiO_2 nanotube array
Fe incorporation
Ultrasound-assisted impregnation
Photocatalytic activity
Visible-light

ABSTRACT

Fe incorporated TiO_2 nanotube arrays (Fe–TiO_2NTs) were prepared by an ultrasound-assisted impregnating-calcination method. Scanning electron microscopy (SEM), transmission electron microscopy (TEM), X-ray diffraction (XRD), X-ray photoelectron spectroscopy (XPS), and UV–vis diffuse reflectance spectroscopy (DRS) indicated that α-Fe_2O_3 nanoparticles were deposited into the TiO_2 nanotubes, and in the mean time, some Fe^{3+} ions were doped into TiO_2 lattice. The absorption of Fe–TiO_2NTs in the visible light region increased with the increase of Fe content. The photocatalytic activity of Fe–TiO_2NTs was evaluated by the degradation of methylene blue aqueous solution under visible light irradiation. The results demonstrated that the Fe–TiO_2NTs exhibited significantly enhanced photocatalytic activity compared with pure TiO_2NTs. Photoluminescence (PL) and electrochemical impedance spectroscopy (EIS) analyses further confirmed that the increased photocatalytic activity of the Fe–TiO_2NTs was attributed to an enhanced separation and transfer of photogenerated charge carriers.

1. Introduction

In the last decade, self-organized and vertically oriented TiO_2 nanotube arrays (TiO_2NTs), first synthesized by Grimes and co-workers in 2001 [1], have attracted much attention due to their unique properties such as highly ordered array structure, high specific surface area, outstanding mechanical and chemical stability and eminent charge-transport properties [2]. As a result, TiO_2NTs have been widely used in many practical fields, such as photodegradation of organic compounds [3,4], photoelectrolysis of water splitting [5,6], dye-sensitized solar cells [7–9], hydrogen storage [10], sensor materials [11], and biomedical applications [12]. However, the efficiency of the photocatalytic degradation is limited by the high recombination rate of photogenerated electrons and holes due to its wide band gap (3.2 eV for anatase and 3.0 eV for rutile). To improve photocatalytic activity and utilize solar energy more efficiently, various strategies including doping with non-metal [13–15] and metal ions [16,17], dye-sensitization [8,18,19], and coupling it with a narrow band gap semiconductor materials [20–23] have been adopted to further increase the efficiency and extend their photoresponse to the visible light region.

Among all reported available candidates, Fe is one of the most suitable for industrial applications considering its low cost and easy preparation. Doping TiO_2 with Fe^{3+} is an effective approach to reduce electron–hole recombination rate and increase photocatalytic efficiency in terms of its semi-full electronic configuration and ion radius close to Ti^{4+}. Many efforts have focused on the preparation and photocatalytic behavior of Fe^{3+}-doped TiO_2 nanoparticle powders or films [24–26], but few reports have so far been found regarding Fe^{3+}-doped TiO_2NTs. We synthesized Fe^{3+}-doped TiO_2NTs directly by the electrochemical anodic oxidation of pure titanium in an HF electrolyte solution containing Fe ions, and the enhanced photocatalytic activity under UV irradiation has been demonstrated [16]. Moreover, Fe_2O_3 is one of the most promising semiconductors and can be used as visible light photocatalyst in industrial applications due to its narrow band gap of 1.9 eV [27], low cost, non-toxicity, and high chemical stability. Its photocatalytic properties have been studied in water splitting [28,29] and photo-degradation of organic dye [30,31]. Misra and co-workers [32] reported the deposition of Fe_2O_3 nanorods inside TiO_2 nanotubes by pulsed electrodeposition technique. The resulting Fe_2O_3/TiO_2 nanorod–nanotube arrays displayed strong absorption in the range of 200–600 nm. Schmuki and co-workers [33] prepared self-organized TiO_2NTs functionalized by Fe_2O_3 nanoparticles that showed an increase of photocatalytic activity for degradation of methyl orange under UV irradiation [31]. Recently, Fe-modified TiO_2NTs prepared by integrating a dip-coating procedure and annealing post-treatment exhibited a larger photocurrent response and higher photoelectrocatalytic activity under visible light irradiation than pure TiO_2NTs [34].

* Corresponding author. Tel.: +86 592 2184655; fax: +86 592 2186657.
E-mail address: sunlan@xmu.edu.cn (L. Sun).

0304-3894/$ – see front matter © 2011 Elsevier B.V. All rights reserved.
doi:10.1016/j.jhazmat.2011.11.031

Ultrasound-driven technology has been widely utilized in physical or chemical processes because it is possible to induce chemical modification on various materials. Recently, CdS incorporated TiO_2NTs [35] and Ag loaded TiO_2NTs [36] have been prepared by a single-step sonoelectrodeposition method and an ultrasonic-assisted photochemical reduction technique, respectively. Cho et al. [22] prepared CdS quantum-dot-sensitized TiO_2NTs by an ultrasound-assisted sequential chemical bath deposition approach and an enhanced photocatalytic activity was found. The ultrasonic is not only able to remove the air trapped in the TiO_2 nanotubes, but also able to drive the solution into the pore networks and lead to a homogeneous adsorption of metal ions on the surface of TiO_2 nanotubes. Here, ultrasonic-assisted impregnating-calcination method was used to prepare the Fe incorporated TiO_2 nanotube arrays (Fe–TiO_2NTs). By this method, which can simplify the synthetic procedures of Fe–TiO_2NTs, Fe_2O_3 nanoparticles can be deposited on the surface of the TiO_2 nanotubes, and in the meantime, Fe^{3+} can be doped into TiO_2 lattice. The amount of the incorporated Fe can be easily adjusted by the ultrasonic time. The photocatalytic activity of the samples was evaluated by the photocatalytic degradation of methylene blue aqueous solution under visible light irradiation. Taking advantage of photoluminescence (PL) and electrochemical impedance spectroscopy (EIS) techniques, the transfer behavior of photogenerated charges of TiO_2NTs and Fe–TiO_2NTs was investigated.

2. Experimental

2.1. Preparation of Fe–TiO_2NTs

Self-organized, vertically oriented TiO_2NTs layers were prepared directly on Ti foils via electrochemical anodic oxidation in 0.5 wt% HF electrolyte with Pt foil as the counter electrode under 20 V for 30 min as previously described [37,38]. The anodized samples were then rinsed with DI water and dried in air.

Fe–TiO_2NTs samples were prepared using ultrasound-assisted impregnation- calcination method. Typically, TiO_2NTs samples were immersed in 0.01 M $Fe(NO_3)_3{\cdot}9H_2O$ aqueous solution (30 °C) and stimulated immediately by an ultrasonic generator (KQ2200DB, Kunshan Ultrasonic Instrument Co., Ltd.) with frequency of 40 kHz and ultrasonic intensity of 2.4 kW m^{-2} for different times, and dried in air. The samples were subsequently annealed at different temperature in ambient condition for 2 h with heating rate of 5 °C min^{-1} and naturally cooled to induce crystallization.

2.2. Characterization of Fe–TiO_2NTs

The morphologies of the samples were examined using a field emission scanning electron microscope (FE-SEM) (Hitachi S4800). The crystalline structure was identified by transmission electron microscopy (TEM) (JEM 2100) and X-ray diffraction (XRD) (Phillips, Panalytical X'pert, Cu Kα radiation (λ = 1.5417 Å)). The chemical composition of the samples was analyzed by X-ray photoelectron spectroscopy (XPS) (VG, Physical Electrons Quantum 2000 Scanning ESCA Microprobe, Al Kα radiation). The binding energies were normalized to the signal for adventitious carbon at 284.8 eV. UV–vis diffuse reflection spectroscopy (DRS) was recorded using a Varian Cary-5000 spectrophotometer. Photoluminescence measurements were performed on a fluorescence spectrophotometer (Hitachi F-7000) with xenon lamp as excitation source (λ_{ex} = 360 nm). Electrochemical impedance spectroscopy spectra were measured by applying an AC voltage of 10 mV amplitude within the frequency range of 10^5–10^{-2} Hz in 0.1 mol L^{-1} Na_2SO_4 aqueous solution with a sample as a working electrode, Pt wire as a counter electrode, and the saturated calomel electrode (SCE) as a reference electrode. The open circuit potential applied to the working electrode is 0 V (vs. SCE).

2.3. Photocatalytic measurement

The visible-light photocatalytic activity experiments on the TiO_2NTs before and after Fe incorporation were performed by the degradation of the methylene blue (MB) dye in a home-made quartz glass reactor. The reactor was equipped with a water jacket to control the reaction temperature. The distance between the light source and the sample was 10 cm. A 500 W tungsten–halogen lamp was used as visible light source to provide a light intensity of 130 mW cm^{-2}. Before the photocatalytic degradation, the samples (1 cm × 1 cm) were soaked in 30 mL of 13.5 mg L^{-1} MB aqueous solution at 30 °C with continuous stirring by thermostatic water cycle system while bubbling with air for 1 h to reach adsorption equilibrium. After visible-light irradiation started, the solution periodically taken from the reactor was analyzed with a UV–vis spectrophotometer (Unico UV-2102 PC, USA). The analytical wavelength selected for optical absorbance measurement was 664 nm.

3. Results and discussion

3.1. Morphological characterization

Fig. 1a shows a representative scanning electron microscopy (SEM) image of the as-synthesized TiO_2NTs. It can be clearly seen that the self-organized TiO_2 layer consists of a compact array of vertically aligned nanotubes. The inset in Fig. 1a shows the nanotube diameter distribution. The tube diameter was found to be in the range of 60–120 nm, and the average diameter was 96 nm. It is observed from Fig. 1b that the tube length was about 450 nm. After dipping the TiO_2NTs in $Fe(NO_3)_3{\cdot}9H_2O$ aqueous solution in an ultrasonic condition, the air trapped in the TiO_2 nanotubes could be removed. In the meantime, $Fe(NO_3)_3$ solution was also driven into the pore networks, and thus leading to a homogeneous adsorption of Fe^{3+} onto the surface of the TiO_2 nanotubes. As the deposition reaction proceeded, some Fe^{3+} ions gradually hydrolyzed into $Fe(OH)_3$ colloid adhered to the surface of the nanotubes. After the dipping process, the samples were annealed at 500 °C for 2 h. During the annealing process, $Fe(OH)_3$ was dehydrated into Fe_2O_3, and the superfluous Fe^{3+} ions were doped into the lattice of TiO_2. The Fe–TiO_2NTs were finally formed. Fig. 1c–e show the SEM images of TiO_2NTs after ultrasound-assisted impregnating in $Fe(NO_3)_3$ solution for 5, 10 and 20 min, respectively, followed by annealing at 500 °C. Only few iron oxide nanoparticles were deposited onto the surface of the nanotubes for the sample with 5 min impregnating (Fig. 1c). As the ultrasonic time prolonged, the amount of iron oxide nanoparticles gradually increased (Fig. 1d). When the ultrasonic time was increased to 20 min, the iron oxide nanoparticles with size of 10–20 nm were uniformly deposited on the top of the nanotubes (Fig. 1e and f). The corresponding cross-sectional SEM image (Fig. 1g) shows that the iron oxide nanoparticles were also deposited onto the walls of TiO_2 nanotubes (marked with arrows). No obvious damage to the ordered tubular structure of TiO_2NTs can be observed. The incorporation of Fe in/on TiO_2NTs was further demonstrated by the energy diffraction spectrum (EDX) which exhibited the presence of Fe element in the bulk of the TiO_2NTs besides Ti and O (Fig. 1h).

3.2. Crystalline structure characterization

The crystalline structure of the obtained Fe–TiO_2NTs was characterized by TEM. Fig. 2a and b show the top and cross-sectional TEM images of Fe–TiO_2NTs, respectively. Clearly, iron

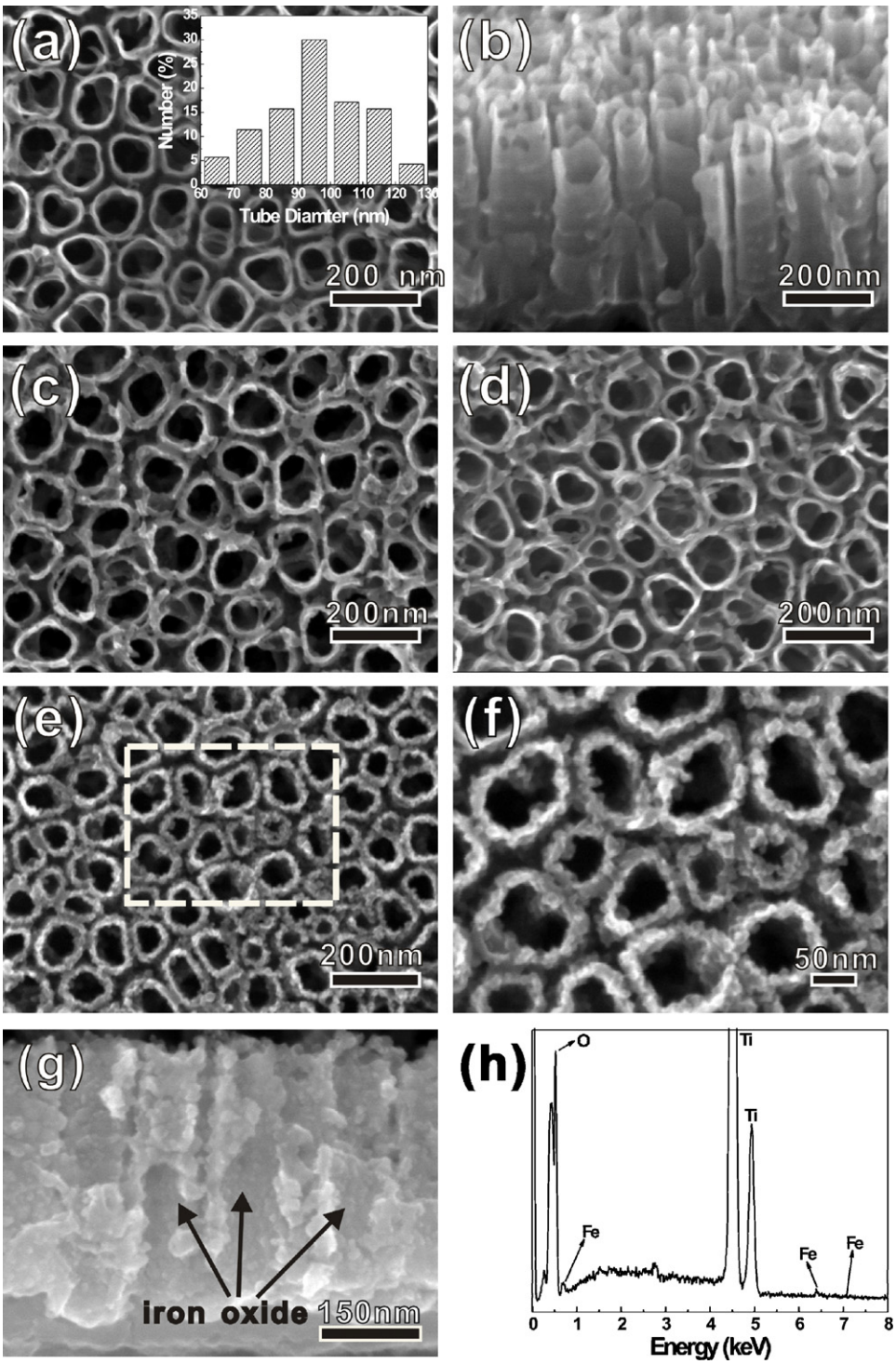

Fig. 1. SEM images of TiO_2NTs (a) and (b) and Fe–TiO_2NTs after ultrasound-assisted deposition in $Fe(NO_3)_3{\cdot}9H_2O$ solution for 5 min (c), 10 min (d), 20 min (e)–(g) and EDS pattern (h). The inset in (a) is the histogram of the nanotube diameter distributions.

oxide nanoparticles were successfully deposited inside the TiO_2 nanotubes. The selected area electron diffraction (SAED) pattern taken from the wall of nanotubes confirmed that annealed TiO_2 nanotubes were polycrystalline in nature (anatase) (inset of Fig. 2b). Some agglomerated nanoparticles were also found (Fig. 2c). HRTEM was used to identify the crystal structure of iron oxide nanoparticles. As we can see from Fig. 2d, the lattice fringes of 0.272 nm corresponded to the (1 0 4) plane of α-Fe_2O_3 (hematite) [39], confirming that iron oxide nanoparticles were crystallized as α-Fe_2O_3.

The crystalline structure of the samples was further analyzed by XRD. Fig. 3a shows the XRD patterns of the TiO_2NTs before and after incorporating Fe. The crystal structure of TiO_2NTs mainly consisted of anatase phase ($2\theta = 25.3^\circ$) and little amount of rutile phase ($2\theta = 27.5^\circ$). After Fe was incorporated into the nanotubes, three additional diffraction peaks were found at 33.3°, 35.8° and 54.2°, in well accordance with the (1 0 4), (1 1 0) and (1 1 6) planes of hematite structure of Fe_2O_3 (α-Fe_2O_3) (JCPDS No. 33-0664), respectively. Fig. 3b shows the enlargement of the XRD patterns

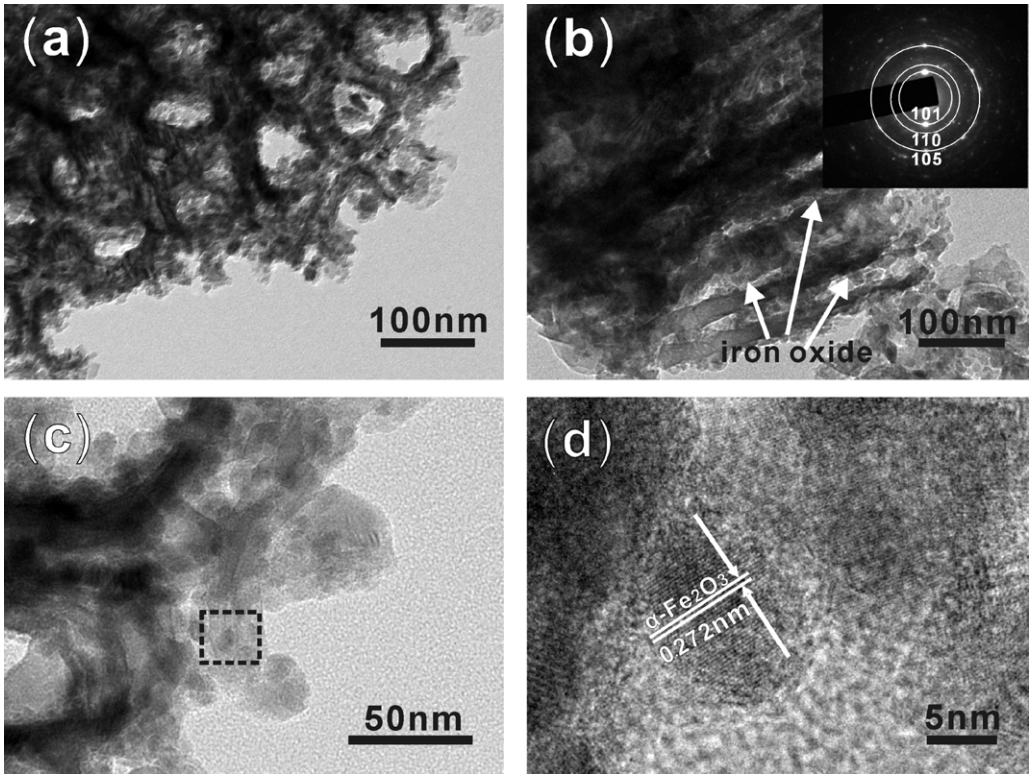

Fig. 2. (a) Low-magnification top view TEM image of Fe–TiO_2NTs. (b) Cross sectional TEM image of Fe–TiO_2NTs. (c) High-magnification top view TEM image of Fe–TiO_2NTs. (d) HRTEM image of the square area in (c). The inset in (b) shows the SAED pattern of nanotubes.

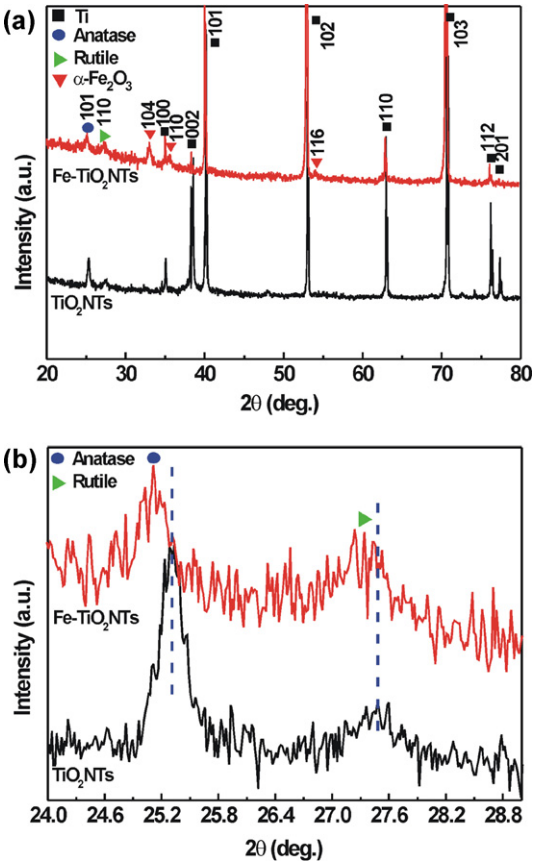

Fig. 3. XRD patterns (a) and regional XRD patterns (b) of TiO_2NTs and Fe–TiO_2NTs.

of TiO_2NTs and Fe–TiO_2NTs in the range from $2\theta = 24.0^\circ$ to 28.8°. Compared with TiO_2NTs, Fe–TiO_2NTs showed the anatase diffraction peak at $2\theta = 25.1^\circ$ and rutile diffraction peak at $2\theta = 27.3^\circ$, respectively. The 0.2° shift of the diffraction peaks may be ascribed to the fact that Fe^{3+} was doped into TiO_2 lattice and formed the Fe–O–Ti bond. Accordingly, after ultrasound-assisted impregnating and annealing, the surface of the TiO_2NTs was modified by α-Fe_2O_3 nanoparticles, and in the meantime, the TiO_2NTs was doped with Fe^{3+}.

Fig. 4a shows XPS survey spectrum of the Fe–TiO_2NTs. The sample contains Ti, O, Fe, and C elements. The C element was ascribed to the adventitious hydrocarbon of the XPS instrument. High-resolution XPS of the Fe element is shown in Fig. 3b. The peaks located at 710.8 and 724.7 eV can be assigned to the Fe $2p_{3/2}$ and the Fe $2p_{1/2}$, respectively, in agreement with that for Fe_2O_3 [40,41]. The main Fe $2p_{3/2}$ and $2p_{1/2}$ peaks were clearly accompanied by weak satellite structures on their high binding-energy side, at about 8 eV above the respective Fe 2p line. It is a typical spectrum of Fe_2O_3 oxides (α- and γ-Fe_2O_3 polymorphs) [41,42]. Fig. 4c and d show the XPS spectra of Ti and O elements, respectively. The peak positions for the Ti 2p core level and O 1s core level of Fe–TiO_2NTs were slightly shifted to lower binding energy. This indicated that Fe^{3+} ions were successfully doped into the substitutional sites of TiO_2 lattice and produced the Fe–O–Ti bond [43].

3.3. UV–vis diffuse reflectance spectra

The effect of Fe incorporating on the light absorption characteristic of TiO_2NTs is shown in Fig. 5. The onset of the absorption for TiO_2NTs is at ca. 390 nm, which is consistent with the intrinsic bandgap absorption of anatase TiO_2 (~3.2 eV). The trapped holes exhibited the absorption at about 410 nm or even shorter, while the

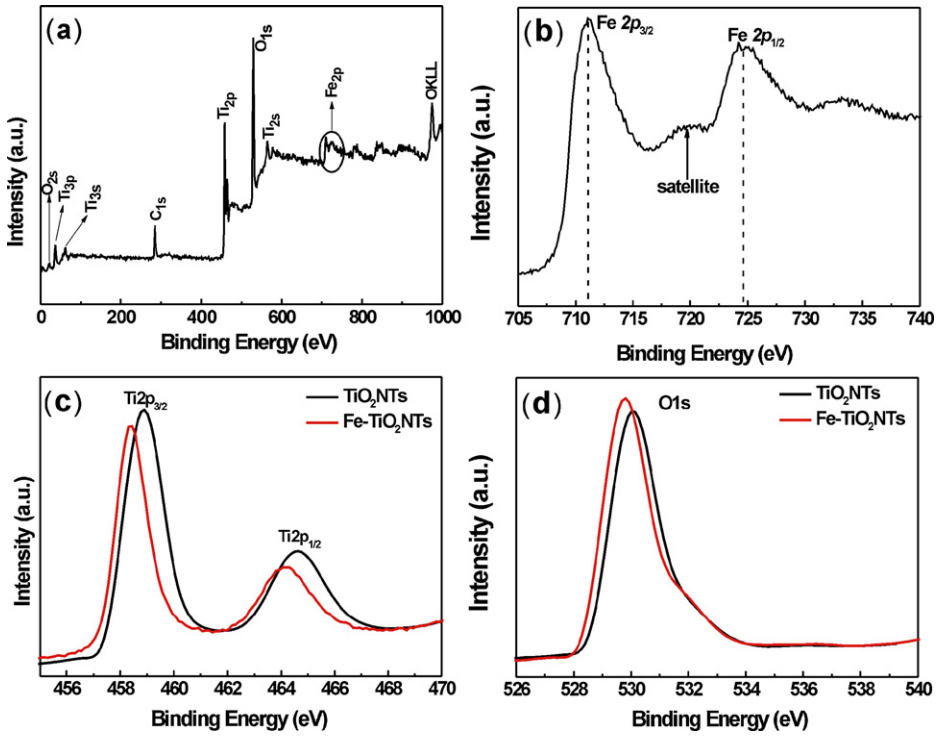

Fig. 4. XPS survey spectrum of Fe–TiO_2NTs (a) and high-resolution XPS spectra of Fe 2p (b), Ti 2p (c) and O 1s (d) of Fe–TiO_2NTs.

trapped electrons showed another absorption at around 540 nm, which was identified to be the sub-bandgap states of the TiO_2NTs [44]. For Fe–TiO_2NTs samples the bandgap edges were shifted toward more the visible-light region (red shift) and the absorption in the visible-light region was significantly enhanced with the increase of the ultrasonic time (i.e., the increase of Fe content). The red-shift of the absorption edge and enhanced visible-light absorption can be attributed to a sub-band-gap transition between the 3d electrons of Fe^{3+} and the TiO_2 conduction or valence band giving rise to a band center at about 400 nm [45,46] and the d–d transition of Fe^{3+} ($2T_{2g} \rightarrow 2A_{2g}$, $2T_{1g}$) or the charge transfer transition between interacting iron ions ($Fe^{3+} + Fe^{3+} \rightarrow Fe^{4+} + Fe^{2+}$) giving rise to an apparent broad band center at 540 nm [45,47,48]. Furthermore, α-Fe_2O_3 nanoparticles deposited on the TiO_2NTs could be easily excited under visible light irradiation and thus would favor the absorption of solar energy in visible light region.

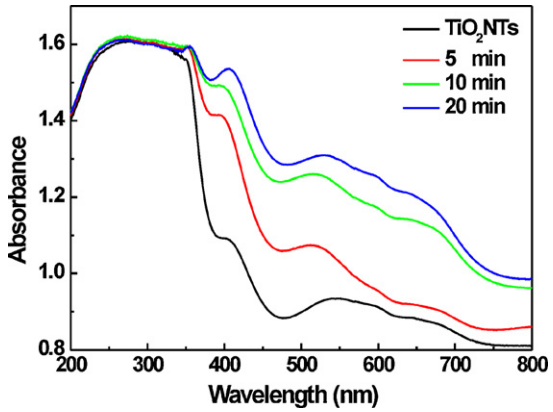

Fig. 5. UV–vis diffuse reflectance spectra of TiO_2NTs and Fe–TiO_2NTs samples prepared under different ultrasonic time.

3.4. Photocatalytic activity

To explore the photoinduced applications of Fe–TiO_2NTs, the photocatalytic activities of a series of samples treated with different ultrasonic time were evaluated by the visible light degradation of MB. Fig. 6a shows the photodegradation kinetics of the MB dye. The photocatalytic reactions for all Fe–TiO_2NTs samples obeyed pseudo first-order reaction kinetics, which could be expressed by $\ln(C/C_0) = -kt$ with k being the apparent first-order reaction constant, while C_0 and C are the initial and the reaction concentrations of the MB dye, respectively. The blank experiment (in absence of TiO_2 photocatalyst) revealed that MB can be decomposed slowly by visible light. The apparent first-order rate constant of the photocatalytic degradation of MB with the assistance of pure TiO_2NTs photocatalyst ($0.00202\ min^{-1}$) was almost the same as that of MB self-degradation ($0.00195\ min^{-1}$). This result demonstrated that TiO_2NTs cannot be sensitized by MB dye under visible light irradiation. An obvious increase of the MB photodegradation was found upon Fe–TiO_2NTs. The inset of Fig. 6a shows the corresponding variation of the apparent first-order reaction constant k as a function of the ultrasonic time. As the ultrasonic time increased, the photocatalytic activity of Fe–TiO_2NTs increased rapidly and reached a maximum value at 5 min. As the ultrasonic time was increased to 20 min, on the contrary, the photocatalytic activity gradually decreased. Obviously, in this case, the optimal ultrasonic time is 5 min, and the photocatalytic activity of the corresponding Fe–TiO_2NTs was increased by a factor of 1.2 compared with that of TiO_2NTs. As the ultrasonic time further prolonged, the amount of incorporated Fe also increased. Once the concentration of Fe^{3+} ions exceeded a certain concentration, Fe^{3+} ions could act as the recombination centers of the photo-generated electrons and holes, resulting in the decrease of photocatalytic activity [42]. Furthermore, a high loading of α-Fe_2O_3 nanoparticles may impede the penetration of the MB solution and the interfacial charge transfer in photocatalytic reaction. Therefore, appropriate Fe^{3+} amount doped in TiO_2 and a low loading of the α-Fe_2O_3 nanoparticles on the

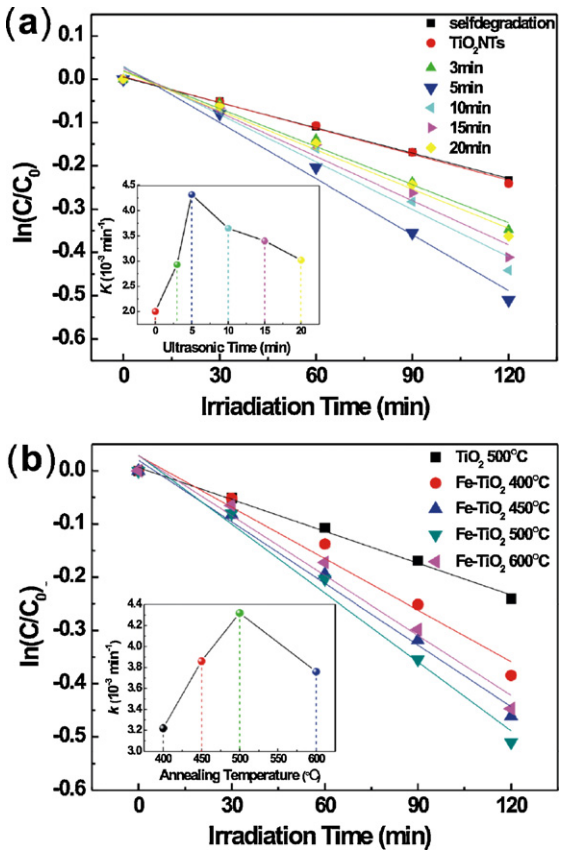

Fig. 6. MB photodegradation kinetic curves of TiO_2NTs and Fe–TiO_2NTs samples prepared under different ultrasonic time (a) and annealing temperature (b).

surface of TiO_2 nanotubes might result in the most enhanced photocatalytic activity. In addition, we compared the photocatalytic activity of the 5 min Fe–TiO_2NTs annealed at different temperature. As shown in Fig. 6b, the optimized efficiency was obtained for the one annealed at 500 °C. We further checked the stability of the 5 min Fe–TiO_2NTs photocatalyst in the reaction medium. The apparent first-order reaction constants of MB photodegradation were reproducible within 5% after 8 photocatalytic cycles, indicating the Fe–TiO_2NTs photocatalyst can remain active for long-term service without much activity degradation.

It is well known that photocatalytic activity is closely related with the lifetime of photogenerated electrons and holes. The separation and recombination processes of photogenerated charge carriers in nano-sized semiconductor materials could be reflected by PL spectrum. Thus, PL spectrum could provide a firm foundation for a quickly evaluation of the photocatalytic activity of semiconductor samples [49]. To confirm the photogenerated charge separation and recombination behaviors in Fe–TiO_2NTs, PL measurement of the Fe–TiO_2NTs with highest photocatalytic activity was carried out and compared with that of TiO_2NTs. As shown in Fig. 7, both Fe–TiO_2NTs and TiO_2NTs exhibited two obvious PL signals with similar curve shape, suggesting that the amount of Fe was not enough to generate a new PL signal. Usually, for anatase TiO_2 materials, there are three types of physical origins: self-trapped excitons, oxygen vacancies and surface state [50–54]. In the present work, both samples displayed a broad-band emission from 400 to 550 nm with two weak shoulder peaks of 417 and 449 nm and an intensive peak of 474 nm. The weak peak position of the 417 nm band can be attributed to radiative recombination of self-trapped excitons [51,55]. Furthermore, the weak peak at 449 nm and the intensive peak at 474 nm can be attributed to oxygen vacancies

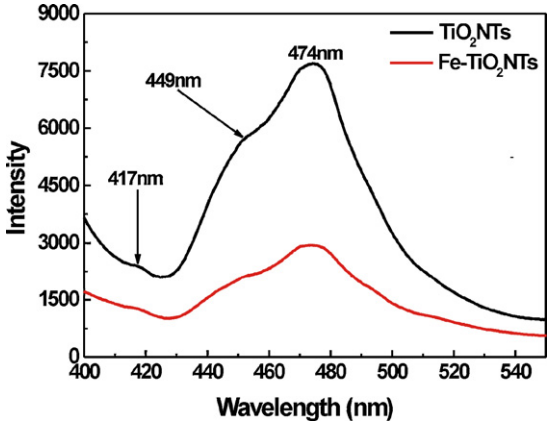

Fig. 7. Room temperature PL spectra of TiO_2NTs and Fe–TiO_2NTs. (Xenon lamp as excitation source, λ_{ex} = 360 nm.)

below conduction band [51,52]. In general, it is believed that a lower excitonic PL intensity means an enhanced separation and transfer of photogenerated electrons trapped in TiO_2 [49]. From the above PL results, Fe–TiO_2NTs showed a relatively low PL intensity. The drastic quenching of PL intensity suggested that Fe incorporated in TiO_2NTs markedly enhanced the charge separation of photogenerated carriers.

As an effective tool for probing the features of surface-modified electrodes, EIS was further employed to analyze the electron transport properties of Fe–TiO_2NTs electrode. Fig. 8 shows Nyquist plots of the EIS spectra measured in 0.1 M Na_2SO_4 aqueous solution under dark and visible light irradiation for the Fe–TiO_2NTs prepared by ultrasonic depositing for 5 min and pure TiO_2NTs. For both TiO_2NTs and Fe–TiO_2NTs, the impedance arc radii in the EIS plane under visible light irradiation were much smaller than that in the dark, implying an improved charge carrier separation under visible light irradiation [56,57]. In particular, the arc radius for Fe–TiO_2NTs electrode was much smaller than that of TiO_2NTs electrode under both dark and visible light irradiation. This result further demonstrated that Fe–TiO_2NTs electrode displayed a much higher separation efficiency of photogenerated electron–hole pairs and faster charge-transfer than TiO_2NTs electrode at the solid–liquid interface. Therefore, incorporating Fe in TiO_2NTs was a promising way to improve the photocatalytic efficiency.

The main charge-transfer processes among TiO_2, Fe^{3+}/Fe^{4+} and α-Fe_2O_3, as shown in Fig. 9, can clarify the enhanced visible light photocatalytic activity of Fe–TiO_2NTs. Since the energy level of Fe^{3+}/Fe^{4+} lies above the valence band edge of anatase TiO_2 [58,59],

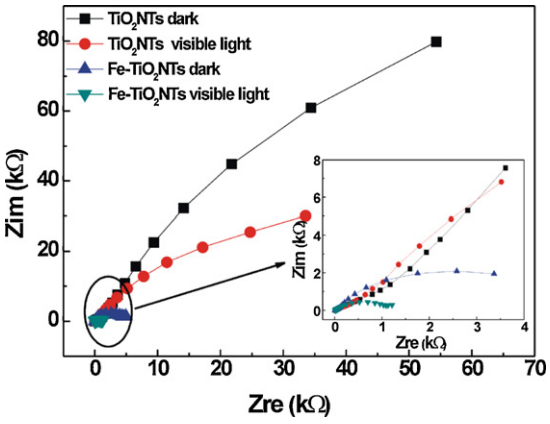

Fig. 8. EIS Nyquist plots of TiO_2NTs and Fe–TiO_2NTs in dark and under visible light irradiation. The inset is the enlargement of the ellipse area.

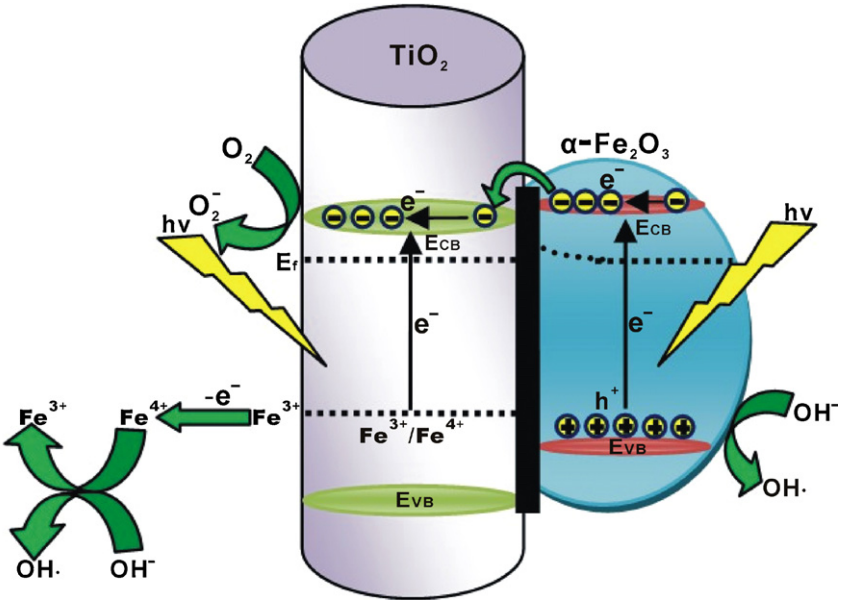

Fig. 9. Schematic illustrating the separation and transport of charge carriers under visible light irradiation for TiO_2NTs, Fe^{3+}/Fe^{4+} and α-Fe_2O_3.

Fe^{3+} doped TiO_2 could absorb visible light. When Fe–TiO_2NTs is irradiated by visible light, a 3d electron may be excited from a Fe^{3+} center to the TiO_2 conduction band leaving behind Fe^{4+} in the energy level of Fe^{3+}/Fe^{4+}. Fe^{4+} can oxidize OH^- in the MB solution to form hydroxyl radicals OH•, while the photogenerated electrons can reduce dissolved oxygen molecules to produce superoxide O_2^- radical anions, which is responsible for the decomposition of MB. In addition, when α-Fe_2O_3 nanoparticles were deposited on the surface of TiO_2 nanotubes, the Fermi levels of TiO_2 and α-Fe_2O_3 must align in equilibrium due to the presence of the α-Fe_2O_3/TiO_2 heterojunction [60,61]. α-Fe_2O_3 could be easily activated and yield charge carriers under visible light irradiation. Subsequently, the photogenerated electrons were immigrated from the conduction band of α-Fe_2O_3 to the conduction band of TiO_2 under the action of built-in electric field and the concentration gradient of electrons, while photogenerated holes were accumulated in the valence band of α-Fe_2O_3. The electrons on the conduction band of TiO_2 can be further transferred to dissolved oxygen molecules to form O_2^-, while the accumulated holes on the valence band of α-Fe_2O_3 could be consumed by participating in reaction with OH^- in the MB solution to produce OH• [61,62]. These active species significantly promoted the photocatalytic oxidation process. Therefore, Fe^{3+} doping combination with α-Fe_2O_3/TiO_2 heterojunction structure are responsible for the efficient photocatalytic activity of Fe–TiO_2NTs.

4. Conclusions

Fe incorporated TiO_2NTs photocatalyst was prepared by a facile ultrasonic-assisted impregnating-calcination method. α-Fe_2O_3 nanoparticles with a size of 10–20 nm were deposited into the TiO_2 nanotubes and some Fe^{3+} ions were doped into TiO_2 lattice. Fe-incorporation induced the red-shift of the absorption edge of TiO_2NTs into the visible-light range. Fe–TiO_2NTs photocatalysts exhibited a much higher visible-light photocatalytic activity for the degradation of MB than TiO_2NTs. The highest degradation efficiency was obtained on the Fe–TiO_2NTs sample prepared by pre-sonicating for 5 min and annealing at 500 °C. In addition, as revealed by PL and EIS, Fe-incorporation effectively promoted the separation and transfer of photogenerated charge carriers, which is responsible for the enhanced photocatalytic activity. The approach described in this study provides a simple and novel method to synthesize Fe–TiO_2NTs materials that are ready for practical applications such as visible-light-driven degradation of wastewater.

Acknowledgments

This work was supported by the National Natural Science Foundation of China (51072170 and 21021002), the Natural Science Foundation of Fujian Province of China (2011J01057) and NFFTBS (J1030415).

References

[1] D.W. Gong, C.A. Grimes, O.K. Varghese, W.C. Hu, R.S. Singh, Z. Chen, E.C. Dickey, Titanium oxide nanotube arrays prepared by anodic oxidation, J. Mater. Res. 16 (2001) 3331–3334.
[2] K.P. Xie, L. Sun, C.L. Wang, Y.K. Lai, M.Y. Wang, H.B. Chen, C.J. Lin, Photoelectrocatalytic properties of Ag nanoparticles loaded TiO_2 nanotube arrays prepared by pulse current deposition, Electrochim. Acta 55 (2010) 7211–7218.
[3] S.P. Albu, A. Ghicov, J.M. Macak, R. Hahn, P. Schmuki, Self-organized, free-standing TiO_2 nanotube membrane for flow-through photocatalytic applications, Nano Lett. 7 (2007) 1286–1289.
[4] J.M Macak, M. Zlamal, J. Krysa, P. Schmuki, Self-organized TiO_2 nanotube layers as highly efficient photocatalysts, Small 3 (2007) 300–304.
[5] J.J. Gong, Y.K. Lai, C.J. Lin, Electrochemically multi-anodized TiO_2 nanotube arrays for enhancing hydrogen generation by photoelectrocatalytic water splitting, Electrochim. Acta 55 (2010) 4776–4782.
[6] S.K. Mohapatra, M. Misra, V.K. Mahajan, K.S. Raja, A novel method for the synthesis of titania nanotubes using sonoelectrochemical method and its application for photoelectrochemical splitting of water, J. Catal. 246 (2007) 362–369.
[7] K. Zhu, N.R. Neale, A. Miedaner, A.J. Frank, Enhanced charge-collection efficiencies and light scattering in dye-sensitized solar cells using oriented TiO_2 nanotubes arrays, Nano Lett. 7 (2006) 69–74.
[8] J. Wang, Z.Q. Lin, Dye-sensitized TiO_2 nanotube solar cells with markedly enhanced performance via rational surface engineering, Chem. Mater. 22 (2009) 579–584.
[9] J.F. Yan, F. Zhou, TiO_2 nanotubes: structure optimization for solar cells, J. Mater. Chem. 21 (2011) 9406–9418.
[10] A. Mishra, S. Banerjee, S.K. Mohapatra, O.A. Graeve, M. Misra, Synthesis of carbon nanotube-TiO_2 nanotubular material for reversible hydrogen storage, Nanotechnology 19 (2008) 445607.
[11] C.X. Wang, L.W. Yin, L.Y. Zhang, R. Gao, Ti/TiO_2 nanotube array/Ni composite electrodes for nonenzymatic amperometric glucose sensing, J. Phys. Chem. C 114 (2010) 4408–4413.
[12] K. Vasilev, Z. Poh, K. Kant, J. Chan, A. Michelmore, D. Losic, Tailoring the surface functionalities of titania nanotube arrays, Biomaterials 31 (2010) 532–540.
[13] N. Lu, X. Quan, J.Y. Li, S. Chen, H.T. Yu, G.H. Chen, Fabrication of boron-doped TiO_2 nanotube array electrode and investigation of its photoelectrochemical capability, J. Phys. Chem. C 111 (2007) 11836–11842.
[14] J.H. Park, S. Kim, A.J. Bard, Novel carbon-doped TiO_2 nanotube arrays with high aspect ratios for efficient solar water splitting, Nano Lett. 6 (2005) 24–28.

[15] Y.N. Huo, Y. Jin, J. Zhu, H.X. Li, Highly active $TiO_{2-x-y}N_xF_y$ visible photocatalyst prepared under supercritical conditions in NH_4F/EtOH fluid, Appl. Catal. B: Environ. 89 (2009) 543–550.
[16] L. Sun, J. Li, C.L. Wang, S.F. Li, H.B. Chen, C.J. Lin, An electrochemical strategy of doping Fe^{3+} into TiO_2 nanotube array films for enhancement in photocatalytic activity, Sol. Energy Mater. Sol. Cells 93 (2009) 1875–1880.
[17] H.J. Liu, G.H. Liu, Q.X. Zhou, Preparation and characterization of Zr doped TiO_2 nanotube arrays on the titanium sheet and their enhanced photocatalytic activity, J. Solid State Chem. 182 (2009) 3238–3242.
[18] T.S. Kang, A.P. Smith, B.E. Taylor, M.F. Durstock, Fabrication of highly-ordered TiO_2 nanotube arrays and their use in dye-sensitized solar cells, Nano Lett. 9 (2009) 601–606.
[19] Z.Y. Liu, V. Subramania, M. Misra, Vertically oriented TiO_2 nanotube arrays grown on Ti meshes for flexible dye-sensitized solar cells, J. Phys. Chem. C 113 (2009) 14028–14033.
[20] M. Sadeghi, W. Liu, T.G. Zhang, P. Stavropoulos, B. Levy, Role of photoinduced charge carrier separation distance in heterogeneous photocatalysis: oxidative degradation of CH_3OH vapor in contact with Pt/TiO_2 and cofumed TiO_2–Fe_2O_3, J. Phys. Chem. 100 (1996) 19466–19474.
[21] Y. Bessekhouad, D. Robert, J.V. Weber, Photocatalytic activity of Cu_2O/TiO_2, Bi_2O_3/TiO_2 and $ZnMn_2O_4$/TiO_2 heterojunctions, Catal. Today 101 (2005) 315–321.
[22] Y. Xie, G. Ali, S.H. Yoo, S.O. Cho, Sonication-assisted synthesis of CdS quantum-dot-sensitized TiO_2 nanotube arrays with enhanced photoelectrochemical and photocatalytic activity, ASC Appl. Mater. Interfaces 2 (2010) 2910–2914.
[23] L.X. Yang, S.L. Luo, Y. Li, Y. Xiao, Q. Kang, Q.Y. Cai, High efficient photocatalytic degradation of p-nitrophenol on a unique Cu_2O/TiO_2 p–n heterojunction network catalyst, Environ. Sci. Technol. 44 (2010) 7641–7646.
[24] X.H. Wang, J.-G. Li, H. Kamiyama, M. Katada, N. Ohashi, Y. Moriyoshi, T. Ishigaki, Pyrogenic iron(III)-doped TiO_2 nanopowders synthesized in RF thermal plasma: phase formation, defect structure, band gap, and magnetic properties, J. Am. Chem. Soc. 127 (2005) 10982–10990.
[25] Z. Ambrus, N. Balázs, T. Alapi, G. Wittmann, P. Sipos, A. Dombi, K. Mogyorósi, Synthesis, structure and photocatalytic properties of Fe(III)-doped TiO_2 prepared from $TiCl_3$, Appl. Catal. B: Environ. 81 (2008) 27–37.
[26] T.Z. Tong, J.L. Zhang, B.Z. Tian, F. Chen, D.N. He, Preparation of Fe^{3+}-doped TiO_2 catalysts by controlled hydrolysis of titanium alkoxide and study on their photocatalytic activity for methyl orange degradation, J. Hazard. Mater. 155 (2008) 572–579.
[27] A. Ghicov, P. Schmuki, Self-ordering electrochemistry: a review on growth and functionality of TiO_2 nanotubes and other self-aligned MOx structures, Chem. Commun. (2009) 2791–2808.
[28] S.U.M. Khan, J. Akikusa, Photoelectrochemical splitting of water at nanocrystalline n-Fe_2O_3 thin-film electrodes, J. Phys. Chem. B 103 (1999) 7184–7189.
[29] J.H. Kennedy, M. Anderman, Photoelectrolysis of water at α-Fe_2O_3 electrodes in acidic solution, J. Electrochem. Soc. 130 (1983) 848–852.
[30] J. Bandara, U. Klehm, J. Kiwi, Raschig rings-Fe_2O_3 composite photocatalyst activate in the degradation of 4-chlorophenol and orange II under daylight irradiation, Appl. Catal. B: Environ. 76 (2007) 73–81.
[31] Y. Wang, C.S. Liu, F.B. Li, C.P. Liu, J.B. Liang, Photodegradation of polycyclic aromatic hydrocarbon pyrene by iron oxide in solid phase, J. Hazard. Mater. 162 (2009) 716–723.
[32] S.K. Mohapatra, S. Banerjee, M. Misra, Synthesis of Fe_2O_3/TiO_2 nanorod–nanotube arrays by filling TiO_2 nanotubes with Fe, Nanotechnology 19 (2008) 315601.
[33] A.I. Kontos, V. Likodimos, T. Stergiopoulos, D.S. Tsoukleris, P. Falaras, I. Rabias, G. Papavassiliou, D. Kim, J. Kunze, P. Schmuki, Self-organized anodic TiO_2 nanotube arrays functionalized by iron oxide nanoparticles, Chem. Mater. 21 (2009) 662–672.
[34] Z.H. Xu, J.G. Yu, Visible-light-induced photoelectrochemical behaviors of Fe-modified TiO_2 nanotube arrays, Nanoscale 3 (2011) 3138–3144.
[35] C.L. Wang, L. Sun, H. Yun, J. Li, Y.K. Lai, C.J. Lin, Sonoelectrochemical synthesis of highly photoelectrochemically active TiO_2 nanotubes by incorporating CdS nanoparticles, Nanotechnology 20 (2009) 295601.
[36] L. Sun, J. Li, C.L. Wang, S.F. Li, Y.K. Lai, H.B. Chen, C.J. Lin, Ultrasound aided photochemical synthesis of Ag loaded TiO_2 nanotube arrays to enhance photocatalytic activity, J. Hazard. Mater. 171 (2009) 1045–1050.
[37] H.F. Zhuang, C.J. Lin, Y.K. Lai, L. Sun, J. Li, Some critical structure factors of titanium oxide nanotube array in its photocatalytic activity, Environ. Sci. Technol. 41 (2007) 4735–4740.
[38] Y.K. Lai, L. Sun, C. Chen, C.G. Nie, J. Zuo, C.J. Lin, Optical and electrical characterization of TiO_2 nanotube arrays on titanium substrate, Appl. Surf. Sci. 252 (2005) 1101–1106.
[39] H. Liu, G.X. Wang, J. Park, J.Z. Wang, H.K. Liu, C. Zhang, Electrochemical properties of α-Fe_2O_3 nanorods as anode material for lithium-ion cells, Electrochim. Acta 54 (2009) 1733–1736.
[40] A.P. Grosvenor, B.A. Kobe, M.C. Biesinger, N.S. McIntyre, Investigation of multiplet splitting of Fe 2p XPS spectra and bonding in iron compounds, Surf. Interface Anal. 36 (2004) 1564–1574.
[41] T. Fujii, F.M.F. de Groot, G.A. Sawatzky, F.C. Voogt, T. Hibma, K. Okada, In situ XPS analysis of various iron oxide films grown by NO_2-assisted molecular-beam epitaxy, Phys. Rev. B 59 (1999) 3195–3202.
[42] G.K. Mor, H.E. Prakasam, O.K. Varghese, K. Shankar, C.A. Grimes, Vertically oriented Ti–Fe–O nanotube array films: toward a useful material architecture for solar spectrum water photoelectrolysis, Nano Lett. 7 (2007) 2356–2364.
[43] L. Pan, J.J. Zou, X.W. Zhang, L. Wang, Photoisomerization of norbornadiene to quadricyclane using transition metal doped TiO_2, Ind. Eng. Chem. Res. 49 (2010) 8526–8531.
[44] Y.K. Lai, L. Sun, Y.C. Chen, H.F. Zhuang, C.J. Lin, J.W. Chin, Effects of the structure of TiO_2 nanotube array on Ti substrate on its photocatalytic activity, J. Electrochem. Soc. 153 (2006) D123–D127.
[45] J.F. Zhu, F. Chen, J.L. Zhang, H.J. Chen, M. Anpo, Fe-TiO_2 photocatalysts prepared by combining sol–gel method with hydrothermal treatment and their characterization, J. Photochem. Photobiol. A: Chem. 180 (2006) 196–204.
[46] T. Umebayashi, T. Yamaki, H. Itoh, K. Asai, Analysis of electronic structures of 3d transition metal-doped TiO_2 based on band calculations, J. Phys. Chem. Solids 63 (2002) 1909–1920.
[47] J.F. Zhu, W. Zheng, B. He, J.L. Zhang, M. Anpo, Characterization of Fe-TiO_2 photocatalysts synthesized by hydrothermal method and their photocatalytic reactivity for photodegradation of XRG dye diluted in water, J. Mol. Catal. A: Chem. 216 (2004) 35–43.
[48] X.Y. Li, P.L. Yue, C. Kutal, Synthesis and photocatalytic oxidation properties of iron doped titanium dioxide nanosemiconductor particles, New J. Chem. 27 (2003) 1264–1269.
[49] L.Q. Jing, Y.C. Qu, B.Q. Wang, S.D. Li, B.J. Jiang, L.B. Yang, W. Fu, H.G. Fu, J.Z. Sun, Review of photoluminescence performance of nano-sized semiconductor materials and its relationships with photocatalytic activity, Sol. Energy Mater. Sol. Cells 90 (2006) 1773–1787.
[50] H. Tang, H. Berger, P.E. Schmid, F. Lévy, G. Burri, Photoluminescence in TiO_2 anatase single crystals, Solid State Commun. 87 (1993) 847–850.
[51] N. Serpone, D. Lawless, R. Khairutdinovt, Size effects on the photophysical properties of colloidal anatase TiO_2 particles: size quantization or direct transitions in this indirect semiconductor? J. Phys. Chem. 99 (1995) 16646–16654.
[52] Y. Lei, L.D. Zhang, G.W. Meng, G.H. Li, X.Y. Zhang, C.H. Liang, W. Chen, S.X. Wang, Preparation and photoluminescence of highly ordered TiO_2 nanowire arrays, Appl. Phys. Lett. 78 (2001) 1125–1127.
[53] J.Y. Shi, J. Chen, Z.C. Feng, T. Chen, Y.X. Lian, X.L. Wang, C. Li, Photoluminescence characteristics of TiO_2 and their relationship to the photoassisted reaction of water/methanol mixture, J. Phys. Chem. C 111 (2006) 693–699.
[54] W.F. Zhang, M.S. Zhang, Z. Yin, Q. Chen, Photoluminescence in anatase titanium dioxide nanocrystals, Appl. Phys. B: Lasers Opt. 70 (2000) 261–265.
[55] X.F. Song, L. Gao, Synthesis, characterization, and optical properties of well-defined N-doped, hollow silica/titania hybrid microspheres, Langmuir 23 (2007) 11850–11856.
[56] Y.K. Lai, H.F. Zhuang, K.P. Xie, D.G. Gong, Y.X. Tang, L. Sun, C.J. Lin, Z. Chen, Fabrication of uniform Ag/TiO_2 nanotube array structures with enhanced photoelectrochemical performance, New J. Chem. 34 (2010) 1335–1340.
[57] Y.K. Lai, J.Y. Huang, H.F. Zhang, V.P. Subramaniam, Y.X. Tang, D.G. Gong, L. Sundar, L. Sun, Z. Chen, C.J. Lin, Nitrogen-doped TiO_2 nanotube array films with enhanced photocatalytic activity under various light sources, J. Hazard. Mater. 184 (2010) 855–863.
[58] Y. Ma, X.T. Zhang, Z.S. Guan, Y.A. Cao, J.N. Yao, Effects of zinc (II) and iron (III) doping of titania films on their photoreactivity to decompose rhodamine B, J. Mater. Res. 16 (2001) 2928–2933.
[59] J.F. Zhu, W. Zheng, B. He, J.L. Zhang, M. Anpo, Characterization of Fe-TiO_2 photocatalysts synthesized by hydrothermal method and their photocatalytic reactivity for photodegradation of XRG dye diluted in water, J. Mol. Catal. A 216 (1) (2004) 35–43.
[60] K.F. Brennan, The Physics of Semiconductors, Cambridge University Press, 1999.
[61] L.L. Peng, T.F. Xie, Y.C. Lu, H.M. Fan, D.J. Wang, Synthesis, photoelectric properties and photocatalytic activity of the Fe_2O_3/TiO_2 heterogeneous photocatalysts, Phys. Chem. Chem. Phys. 12 (2010) 8033–8041.
[62] L.F. Cui, Y.S. Wang, M.T. Niu, G.X. Chen, Y. Cheng, Synthesis and visible light photocatalysis of Fe-doped TiO_2 mesoporous layers deposited on hollow glass microbeads, J. Solid State Chem. 182 (2009) 2785–2790.